Journal of Power Sources 249 (2014) 239–246

Contents lists available at ScienceDirect

Journal of Power Sources

journal homepage: www.elsevier.com/locate/jpowsour

Investigation of carbon supported Pd–Cu nanoparticles as anode catalysts for direct borohydride fuel cell

Gamze Behmenyar [a,b,*], Ayşe Nilgün Akın [b]

[a] TUBITAK, Marmara Research Center, Energy Institute, 41470 Gebze, Kocaeli, Turkey
[b] Kocaeli University, Chemical Engineering Department, 41380 Kocaeli, Turkey

HIGHLIGHTS

- The Pd–Cu/C alloy catalysts represent much higher electrochemical catalytic activity than Pd/C.
- $Pd_{50}Cu_{50}$/C reveals the highest electrochemical performance with small amount of metal loading.
- $Pd_{50}Cu_{50}$/C shows high mass activity 196 W g^{-1} as anode catalyst.
- Pd–Cu/C catalysts seems promising anode catalyst for the DBFC application.

ARTICLE INFO

Article history:
Received 8 June 2013
Received in revised form
8 October 2013
Accepted 16 October 2013
Available online 25 October 2013

Keywords:
Direct borohydride fuel cell
Nanoparticles
Anode catalyst
High performance

ABSTRACT

Carbon supported Pd and bimetallic Pd–Cu nanoparticles with different compositions are prepared by a modified polyol method and used as anode catalysts for direct borohydride fuel cell (DBFC). The physical and electrochemical properties of the as-prepared electrocatalysts are investigated by transmission electron microscopy (TEM), X-ray diffraction (XRD), ICP-AES, cyclic voltammetry (CV), chronoamperometry (CA), and fuel cell experiments. The results show that the carbon supported Pd–Cu bimetallic catalysts have much higher catalytic activity for the direct oxidation of BH_4^- than the carbon supported pure nanosized Pd catalyst, especially the $Pd_{50}Cu_{50}$/C catalyst presents the highest catalytic activity among all as-prepared catalysts, and the DBFC using $Pd_{50}Cu_{50}$/C as anode catalyst and Pt/C as cathode catalyst gives the best performance, and the maximum power density is 98 mW cm^{-2} at a current density of 223 mA cm^{-2} at 60 °C.

1. Introduction

Proton exchange membrane fuel cells (PEMFCs) have attracted growing interest as promising alternative power source for transportation and mobile applications due to high-energy efficiency. However, there are several issues have to be resolved, such as supply, storage and transportation of hydrogen and high stack cost [1,2]. Therefore, certain organic liquid fuels, such as methanol, ethanol, have been considered as an alternative fuel. There are a number of concerns associated with these organic fuels, including low activity, toxicity, and low oxidation efficiency, compared to hydrogen. Direct methanol fuel cells (DMFCs) are the most attractive. But the low cell voltage and power density due to poisoning of the anode during methanol oxidation and methanol crossover limit the application of DMFCs [3]. One solution for this problem is to use sodium borohydride ($NaBH_4$) aqueous solution as fuel because of its high energy density (9296 Wh kg^{-1}), high capacity (5669 Ah kg^{-1}) and high hydrogen content of about 11 wt%. Moreover, sodium borohydride is easily stored and distributed, chemically stable and the resulting metaborate environmentally acceptable and can be recycled to sodium borohydride. These advantages of $NaBH_4$ accelerated the search on direct borohydride fuel cell, especially for portable application [4,5].

The reactions in borohydride fuel cells are:

Anode reaction is the electro-oxidation of borohydride ion to release $8e^-$ according to the following reaction [6]:

$$BH_4^- + 8OH^- \rightarrow BO_2^- + 6H_2O + 8e^-, \quad E^0 = -1.24\ \text{V vs. SHE} \tag{1}$$

Cathode:

$$2O_2 + 4H_2O + 8e^- \rightarrow BO_2^- + 6H_2O + 8e^-, \quad E^0 = 0.4\ \text{V vs. SHE} \tag{2}$$

* Corresponding author. TUBITAK, Marmara Research Center, Energy Institute, P.O. Box 21, 41470 Gebze, Kocaeli, Turkey. Tel.: +90 262 677 27 11; fax: +90 262 64123 09.
E-mail address: Gamze.Behmenyar@Tubitak.gov.tr (G. Behmenyar).

0378-7753/$ – see front matter © 2013 Elsevier B.V. All rights reserved.
http://dx.doi.org/10.1016/j.jpowsour.2013.10.063

Overall:

$$BH_4^- + 2O_2 \rightarrow BO_2^- + 2H_2O + 8e^-, \quad E^0_{cell} = 1.64\ V\ vs.\ SHE \tag{3}$$

In the electrochemical oxidation of sodium borohydride, the electrocatalyst is a key material. Studies have been conducted on a wide range of anode catalysts such as noble metals (Pt, Pd, Au, Ag) [7–11], and transition metals (Cu, Ni) [12,13] in order to assess their effect on borohydride oxidation and cell performance. The complete oxidation of borohydride release eight electrons ($8e^-$) per molecule in theory (Eq. (1)), while in practice $8e^-$ are only obtained by using an Au anode catalyst. However, the slow electrode kinetics of BH_4^- on the Au electrode results in low current and power output [14]. Anode materials such as Pt and Pd demonstrate fast electrode kinetics and thus good power performances. However, high costs of such noble metal significantly increase the total price of catalysts. It is known that bimetallic or alloy catalysts show higher catalytic activity and stability than monometallic ones. Noble metal–nonnoble metal alloy might be the best alternative to the economical catalyst with desired performance. As a nonnoble metal, 3d transition metals (Fe, Co, Ni, Cu, Zn), which are cheaper than palladium and platinum, are good candidates to catalyze anodic reactions of sodium borohydride. Carbon supported Pt and Pt-alloys were investigated as anode catalyst by Gyenge et al. It was found that Pt–Ni/C gave the higher cell voltage than Pt/C and Pt–Au/C [15]. Tegou et al. studied electrochemical oxidation of borohydride at Pt, Pt–Ni, Pt–Co and AuPt(Ni) electrodes and reported that these bimetallic catalysts showed promising activity towards borohyride oxidation [16,17]. Yi and co-workers prepared Pt/C and Pt–Cu/C catalysts and found that Pt–Cu/C catalyst represented much higher electrochemical catalytic activity for BH_4^- oxidation than Pt/C and long term running stability [18]. Especially $Pt_{50}Cu_{50}$/C showed the highest electrocatalytic activity to the direct oxidation of BH_4^- and they concluded that $Pt_{50}Cu_{50}$/C would be a promising catalyst to make less-expensive fuel cell. Wang at al. [19–23] prepared Au–M (M = Fe, Co, Ni, Cu and Zn) nanoparticles and used as the anode catalyst. All AuM/C catalysts showed higher activity for BH_4^- oxidation than that of pure Au/C catalyst.

Palladium shows fast electrode kinetics and good power performance and relatively cheap comparing with Platinum. Alloying Pd with a transition metal such as Cu can reduce the cost of catalyst and keep or even improve the catalytic activity for BH_4^- oxidation and power output. To the author's knowledge, there is no information available in literature about electrooxidation of BH_4^- on the carbon supported Pd–Cu bimetallic nanoparticles. In the present study, a series of Pd–Cu bimetallic nanoparticles supported on carbon black Vulcan XC-72 were prepared by a modified polyol method. The performances of the prepared catalysts were evaluated in detail by cyclic voltammetry, chronoamperometry and fuel cell measurements.

2. Experimental methods

All chemical reagents were of analytical grade: Palladium(II) acetate (for synthesis) Merck, copper(II) acetate 99.9%(metals basis) Alfa Aesar, Nafion solution (5 wt%) Alfa Aesar, and 1,4 Dioxane ACS, 99% Alfa Aesar. Other chemicals, such as ethanol (ACS reagent grade), methanol (ACS reagent grade) 99.9% and Ethylene glycol >99% were purchased from Merck. Carbon black (Vulcan XC-72, Cabot) was used as the nanoparticle support material.

2.1. Synthesis of catalysts by polyol method

PdCu/C bimetallic alloy catalysts were prepared by modified polyol method developed by our group without using any stabilizer. Palladium acetate and copper acetate, ($PdII(OAc)_2$ and $CuII(OAc)_2$), were used as metal precursors in controlled molar ratios and ethylene glycol as reducing agent. All catalysts were prepared with 20 wt% metal loading on Vulcan XC-72 carbon support. Calculated amount of $PdII(OAc)_2$ and $CuII(OAc)_2$ were dissolved in dioxan and ethylene glycol respectively and added to pretreated carbon and ethylene glycol solution. The pH value of the solution is increased to above 9 with the solution of sodium hydroxide in water, and the solution is stirred for 1 h at room temperature and subsequently heated under reflux to predetermined temperature for 2 h. The resulting suspension was cooled down quickly by using ice bath. Carbon supported catalysts were then filtered and extensively washed with ethanol and distilled water, followed by drying under very high vacuum at 25 °C.

2.2. Physical characterization of Pd–Cu/C electrocatalysts

The structure and morphology of the prepared electrocatalysts were examined by transmission electron microscopy analysis. Transmission Electron Microscopy measurements were performed on JEOL JEM 2100 HRTEM operating at 200 kV (LaB6 filament) with Oxford Instruments X-Sight 6498 EDS system. Images were taken by Gatan Model 694 Slow Scan CCD Camera. After dissolving the catalysts with ethanol, very small amount of samples were dropped onto carbon support film coated copper TEM grids (EMS, 200 meshes).

X-ray diffractometer (Philips PW3710 PANalytical X'Pert PRO MPD model) was employed with Cu Ka radiation (l = 1.54056 Å) to obtain X-ray diffraction (XRD) patterns of the samples. The 2θ angular regions between 2° and 80° were explored at a scan rate of 1° min^{-1}.

2.3. Electrochemical measurements

The Pd–Cu/C or Pd/C was used as working electrode, a carbon road as counter electrode and an Ag/AgCl, KCl std as the reference electrode. The electrolyte was 0.03 M $NaBH_4$ + 3.0 M NaOH. The working electrode was prepared as follows: the catalyst powder (10 mg) is added to a mixture of Nafion solutions in ethanol. After ultrasonic homogenization of the catalyst ink for 2 h, a given amount of volume is deposited onto the glassy carbon (GC) electrode (3 mm in diameter) which was polished by 0.5 μ alumina and sonicated 5 min prior to use. The ink is then evaporated in a mild stream of ultrapure nitrogen for 3 h at room temperature. The loading mass of catalyst was 0.7 mg cm^{-2} and actual metal loading mass on the electrode is 0.14 mg cm^{-2}. Electrochemical measurements were performed using Gamry Workstation and a typical three-electrode one compartment electrolysis cell.

2.4. Fuel cell performance tests

The electrocatalyst ink was prepared by mixing methanol with 5 wt% Nafion solution and carbon-supported catalysts. Then, the ink was coated on a carbon cloth (Electrochem, Inc.), yielding a metal loading mass on the electrode of 0.5 mg cm^{-2}. The Nafion-115 membrane was cleaned by boiling in 3 wt% H_2O_2 and for 1 h, followed by boiling in ultrapure water for 1 h. The cleaned membrane was activated by boiling in 2 M NaOH solution for 1 h prior to use. The anode/membrane/cathode unit was compressed between two graphite block current collectors with a single serpentine flow field with rectangular channels 1 mm wide and 1 mm deep. Silicon gaskets were assembled between the electrode and the graphite block. The active area within the fuel cell was 25 cm^2. Cell performance was tested against a 0.5 mg cm^{-2} Pt/C cathode. Peristaltic pumps were used to feed the fresh anolyte (an aqueous solution of

1 M $NaBH_4$ and 6 M NaOH) at a 3 cm^3 min^{-1} flow rate. The flow rate of oxidant at the cathode chamber was 0.2 l min^{-1}. The oxidant was humidified by passing through a bubbler at 65 °C. Cell performance data were obtained using an electrochemical fuel cell test system (Electrochem 400 W) and a computer-controlled E-load system (ECL 150).

3. Results and discussion

3.1. Physical characterization

The atomic composition of the Pd_nCu_{100-n}/C alloys was confirmed by inductively coupled plasma optical emission spectroscopy (ICP-OES). The atomic percentages of Pd metal in $Pd_{75}Cu_{25}$/C, $Pd_{50}Cu_{50}$/C and $Pd_{25}Cu_{75}$/C samples obtained from ICP-AES data are 76, 49 and 27 respectively. All Pd–Cu catalysts present atomic percentages very close to expected value, which confirm that metals were completely reduced during the synthesis process, but this method cannot provide any information about the microstructure of the formed alloys. Therefore, XRD measurements were performed in order to evaluate the microstructure of the prepared catalysts. Fig. 1 shows the XRD patterns of the Pd/C, $Pd_{75}Cu_{25}$/C, $Pd_{50}Cu_{50}$/C and $Pd_{25}Cu_{75}$/C catalysts. The wide diffraction peak in all patterns positioned at a 2θ value of about 25.0° is attributed to the Vulcan XC-72 carbon (002) crystal face, which matches with the standard C peak (JCPDS75-1621). For monometallic Pd/C catalyst (Fig. 1a), the peaks positioned at 2θ values of 39.9°, 46.2° and 67.8° could be indexed to the (111), (200), (220), planes of face-centered cubic (fcc) Pd, which could be matched well with the pure Pd peaks (JCPDS-ICDD 46-1043).

XRD patterns of $Pd_{75}Cu_{25}$/C, $Pd_{50}Cu_{50}$/C and $Pd_{25}Cu_{75}$/C catalysts display an asymmetric peak from the (111) reflection centered between the known (111) reflections of pure Pd (40.1°) and Cu (43.4°)(Cu JCPDS-ICDD 4-9-2090) phases, which indicates that bimetallic PdCu alloy structures are formed. No diffraction peaks of Cu or its oxides/hydroxides are observed even with high Cu content $Pd_{25}Cu_{75}$/C catalysts, which is also an indication of Pd atom and Cu atom are alloyed well. The 2θ values of the (111) reflection peaks are 40.91°, 41.7°, and 42.44° for $Pd_{75}Cu_{25}$/C, $Pd_{50}Cu_{50}$/C and $Pd_{25}Cu_{75}$/C catalysts, respectively. These are very close to the expected values of 41.04°, 41.66°, and 42.3° for $Pd_{75}Cu_{25}$/C, $Pd_{50}Cu_{50}$/C and $Pd_{25}Cu_{75}$/C respectively, which were calculated based on Vegard's law [24].

The Scherrer's equation is used to estimate average particle size of the catalysts:

$$D = 0.9\lambda/B\cos\theta$$

where D is the average particle size, nm, λ is the X-ray wavelength (1.54056 Å for Cu Ka radiation), B is the full width at half-maximum in radians (FWHM) and θ is the angle of (111) peak. The calculated average particle size of Pd/C, $Pd_{75}Cu_{25}$/C, $Pd_{50}Cu_{50}$/C and $Pd_{25}Cu_{75}$/C catalysts are 4.45 nm, 2.64 nm, 2.57 nm and 7.5 nm, respectively.

The size of nanoparticles and their dispersion on the support were observed by TEM. Because the preparation methods of PdCu/C catalysts were identical, the $Pd_{50}Cu_{50}$/C catalyst was chosen as the representative to analysis. Fig. 2(a) and (b) is the TEM and HR-TEM images of the $Pd_{50}Cu_{50}$/C catalysts. It can be seen that the metal nanoparticles with a narrow particle size distribution are uniformly dispersed on the surface of carbon. The morphologies of the metal nanoparticles are generally spherical, and the mean particle diameter is approximately 3.5 nm.

TEM mapping images for the PdCu sample, Fig. 3, shows a uniform elemental Cu and Pd distribution in the particle of the mapped area. Therefore, these results agree with those reported for typical electrocatalyst analysis, and suggest that the PdCu/C synthesis method is suitable.

3.2. Electrochemically active surface area estimation

The electrochemically active surface areas (ECSA) of the prepared electrocatalysts were calculated by cyclic voltammetry by considering the zone of surface oxide reduction. The active surface areas of palladium catalysts are characterized by the quantification of the electric charge involved in the reduction of the first PdO monolayer formed on the metal surface, as described by Grdén et al. [25]. The reported charge density associated to the reduction of the formed PdO monolayer is of 424 μC cm^{-1}. Fig. 4 presents cyclic voltammograms recorded from −1 V to 0.5 V at a sweep rate of 20 mV s^{-1} in a N_2-saturated 3 M NaOH solution. PdCu/C alloy catalysts show common potential regions for the reduction of

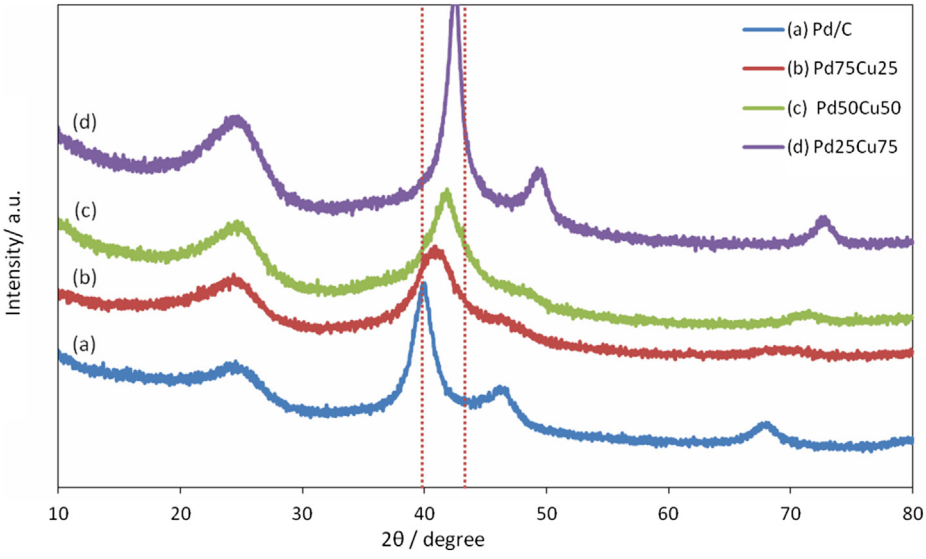

Fig. 1. XRD patterns of Pd–Cu/C with different proportion of Cu dispersed on carbon. Vertical line indicate 2-Theta positions for pure crystalline phases, 40.1° for Pd; 43.4° for Cu.

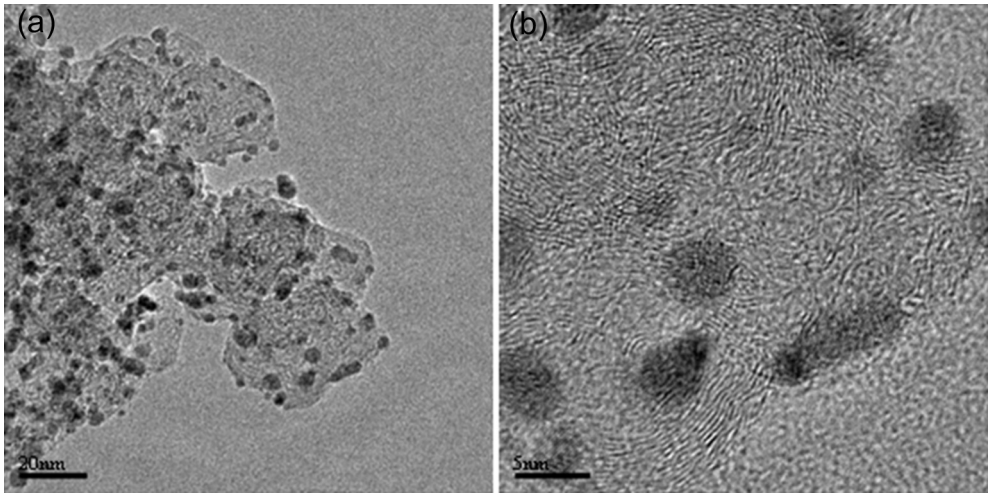

Fig. 2. TEM (a) and HR-TEM (b) images of $Pd_{50}Cu_{50}$ nanoparticles dispersed on carbon.

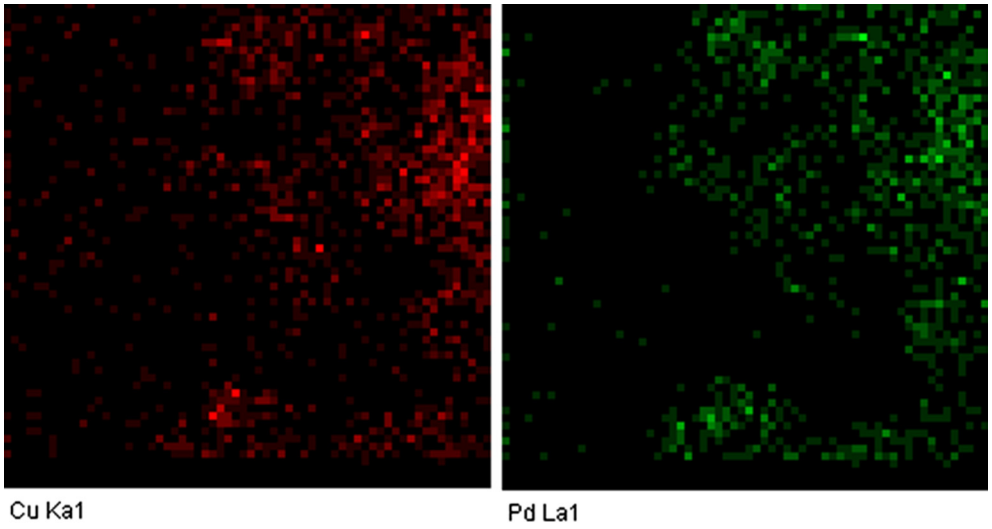

Fig. 3. Images of TEM mapping for the as-synthesized $Pd_{50}Cu_{50}$ electrocatalyst sample.

surface oxide. As the cupper content increased the peak potential goes more negative regions where copper oxide reduction peak occurs. The value of the active surface areas obtained by integration of the oxide reduction zones on the voltammograms [26]. The calculated ECSAs of the Pd/C, $Pd_{75}Cu_{25}$/C, $Pd_{50}Cu_{50}$/C and $Pd_{25}Cu_{75}$/C are 591 $cm^2\ mg^{-1}$, 730 $cm^2\ mg^{-1}$, 1849 $cm^2\ mg^{-1}$, and 483 $cm^2\ mg^{-1}$, respectively. And among the four electrocatalysts, $Pd_{50}Cu_{50}$/C has the highest ECSA, which can be attributed to the smallest and well dispersed PdCu nanoparticles loaded on the carbon as seen in Fig. 2.

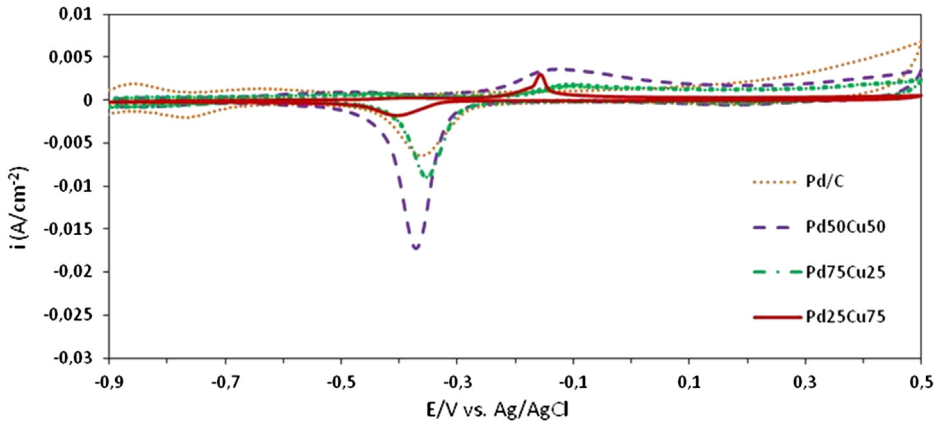

Fig. 4. CV curves of the Pd/C and Pd–Cu/C catalyst in 3 M NaOH at scan rate of 20 mV s^{-1}.

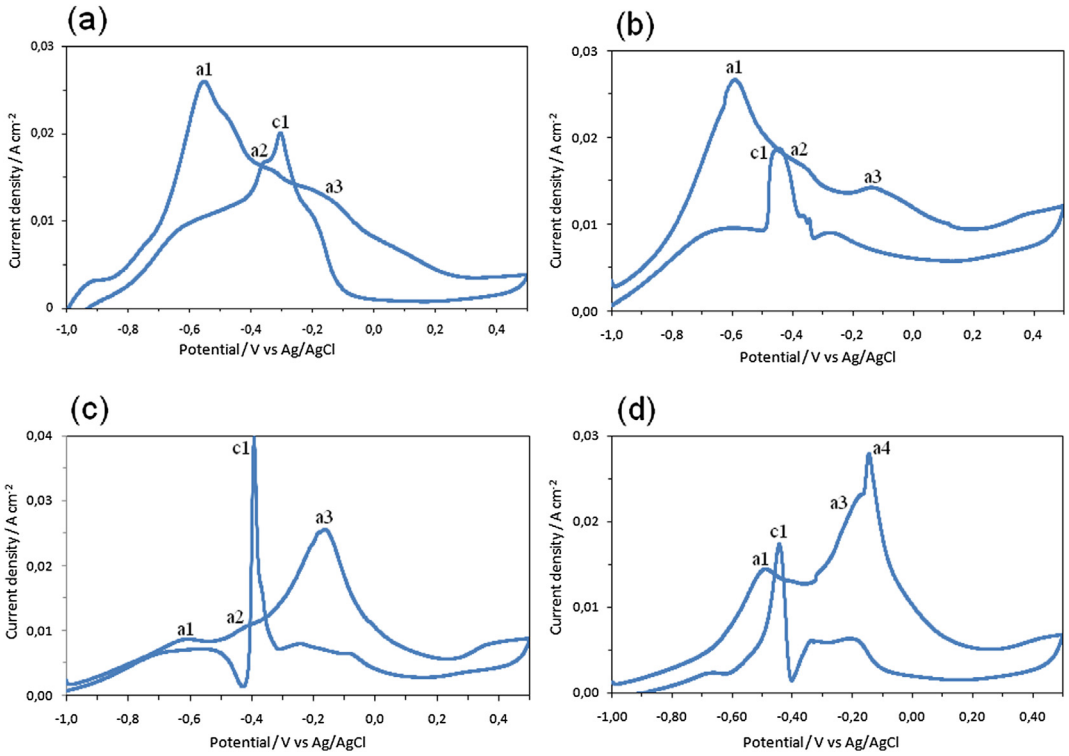

Fig. 5. Cyclic voltammogram plotted on (a) Pd/C, (b) $Pd_{75}Cu_{25}$/C, (c) $Pd_{50}Cu_{50}$/C and (d) $Pd_{25}Cu_{75}$/C in 0.03 M $NaBH_4$ + 3 M NaOH solution at a scan rate of 20 mV s^{-1}.

3.3. Cyclic voltammetry

The cyclic voltammetries recorded using Pd/C, $Pd_{75}Cu_{25}$/C, $Pd_{50}Cu_{50}$/C and $Pd_{25}Cu_{75}$/C electrodes in 0.03 M $NaBH_4$ + 3.0 M NaOH solution at a scan rate of 20 mV s^{-1} in the potential range of −1 V to 0.5 V vs. Ag/AgCl, KCl std are shown in Fig. 5. This is the first description in the literature, to the author's knowledge, of the BH_4^- cyclic voltammogram on PdCu.

Recorded CV curves are complexes and characterized by several oxidation peaks. For all catalysts, in Fig. 5, during the forward sweep, a well-defined oxidation peak (a1) occurs at about −0.6 V, followed by an oxidation wave (a2) appears in the potential range between −0.4 V and −0.25 V. Third one (a3) occurs at about −0.15 V. By increasing Cu content another peak (a4) was observed for $Pd_{25}Cu_{75}$/C electrode. On the return scan, a sharp anodic peak (c1) is also observed.

The first anodic peak (a1) can be assigned to borohydride hydrolysis (Eq. (4)) followed by the electrooxidation of H_2 (Eq. (5)) [8,10]. The second oxidation peak (a2), between −0.4 and −0.25 V, is attributed to the electrooxidation of BH_3OH^- (Eq. (6)) which is also formed in the catalytic hydrolysis of BH_4^-. Martins et al. [8] have observed a similar wave between −0.62 and −0.3 V on Pt in 3 M NaOH, Okinaka [27] between −0.62 and −0.3 V (on Au in 0.2 M KOH), and Gyenge [10] between −0.45 and −0.20 V (on Pt in 2 M NaOH).

$$BH_4^- + H_2O \rightarrow BH_3OH^- + H_2 \quad (4)$$

$$\frac{1}{2}H_2 + OH^- \rightarrow H_2O + e^- \quad (5)$$

$$BH_3OH^- + 3OH^- \rightarrow BO_2^- + 3/2H_2 + 2H_2O + 3e^- \quad (6)$$

At more positive potentials in the forward scan, a third anodic peak a3 appears at about −0.13 V attributed to direct potentially eight-electron oxidation of BH_4^- (Eq. (1)). The direct oxidation peak potential has been reported by Martins et al. [8] at about −0.13 V on Pt in 3 M NaOH, Gyenge [10] has obtained a peak between −0.15 and −0.05 V on Pt in 2 M NaOH, and Okinaka [27] between −0.15 and −0.05 V on Au in 0.2 M KOH.

During the reverse scan, an oxidation peak is observed at about −0.4 V due to the oxidation of BH_3OH^- formed as an intermediate during the oxidation of BH_4^- in the forward reaction [28]. In addition, for the CV curve of $Pd_{25}Cu_{75}$/C electrode (Fig. 5d), the anodic peaks a4 represents formation of CuO [18]. It is observed at −0.15 V which has the same potential as the direct oxidation peak (a3).

It can be seen from Fig. 5c that current densities of peak a1 and a2, coming from BH_4^- hydrolysis, are much lower for $Pd_{50}Cu_{50}$/C

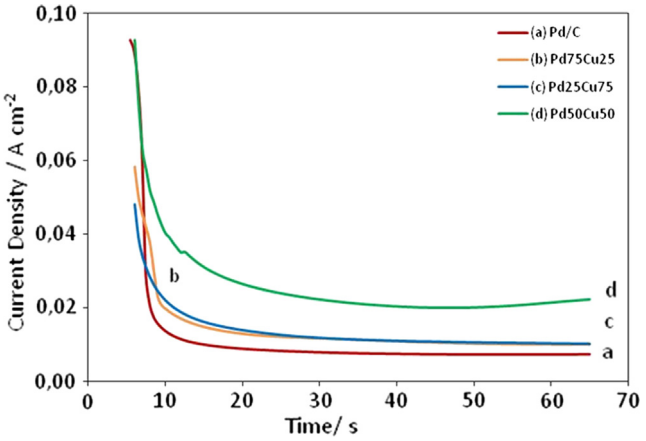

Fig. 6. Chronoamperometry curves of Pd/C and Pd–Cu/C catalyst in 0.03 M $NaBH_4$ + 3 M NaOH solution. Potential step: from −1.2 to −0.2 V vs. Ag/AgCl.

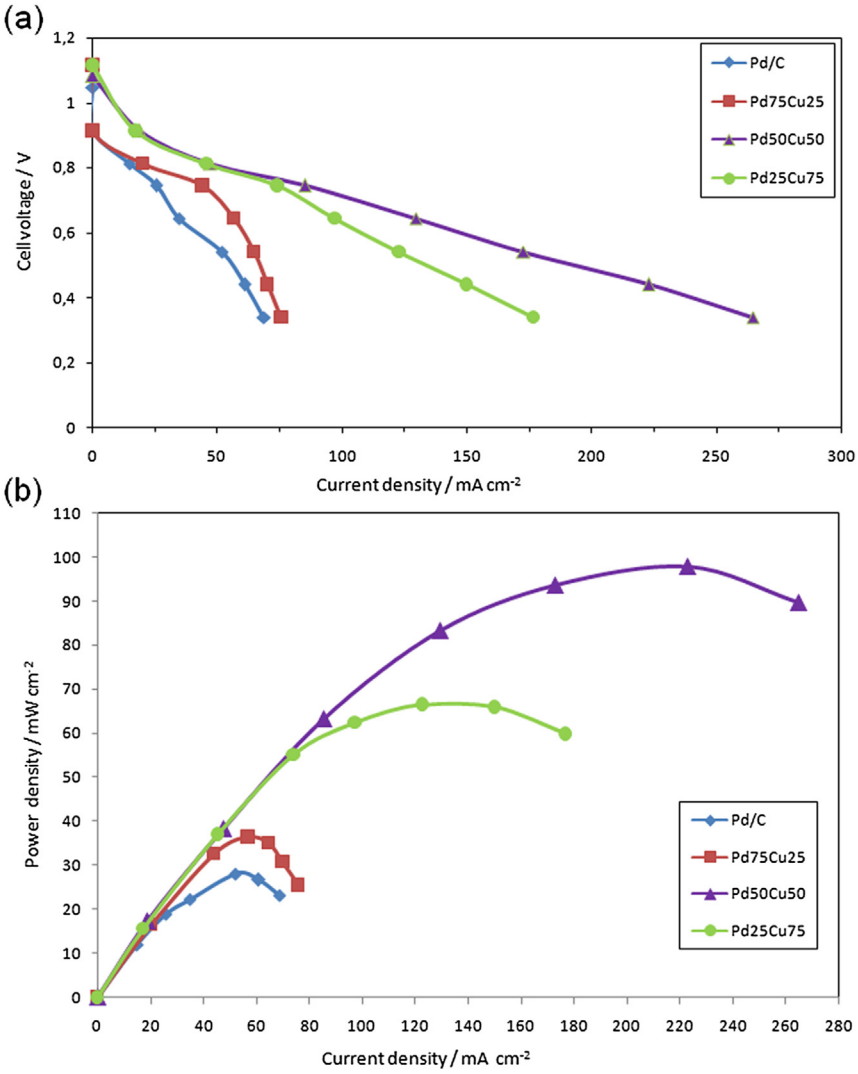

Fig. 7. Cell polarization curves (a) and power density curves (b) of the DBFC using different anode catalysts at 60 °C. Anode loading: 0.5 mg metal cm^{-2}, 3 ml min^{-1} 1 M $NaBH_4$ in 6 M NaOH. Cathode loading: 0.5 mg Pt cm^{-2}, O_2 at 0.2 l min^{-1}.

than the others. On the contrary, current density of the BH_4^- oxidation reaction peak (a3) is the highest for $Pd_{50}Cu_{50}$/C.

All the peak current densities for direct oxidation of BH_4^-, peak a3, on Pd–Cu/C electrodes are higher than that on Pd/C electrode. Among the four electrocatalysts, the peak current density of a3 on the $Pd_{50}Cu_{50}$/C is the highest, 26 mA cm^{-2}, thus the $Pd_{50}Cu_{50}$/C catalyst will show the highest catalytic activity for the electrooxidation of BH_4^-. It can be attributed to the highest active surface area of $Pd_{50}Cu_{50}$/C or synergistic effect of Pd–Cu bimetallic nanoparticles, which jointly improves the electrochemical oxidation of BH_4^- [20].

3.4. Chronoamperometry

Fig. 6 shows the chronoamperometric response of Pd/C, $Pd_{75}Cu_{25}$/C, $Pd_{50}Cu_{50}$/C and $Pd_{25}Cu_{75}$/C electrodes in 0.03 M $NaBH_4$ + 3 M NaOH solution in the case of a potential step from −1.2 to −0.2 V vs. Ag/AgCl, KCl std. As shown in Fig. 6, a decrease in the current density with time was found in each catalyst electrode. In the initial stage ($t < 5$ s) Pd/C and $Pd_{50}Cu_{50}$/C have the highest current density (93 mA cm^{-2}). In three second static current of Pd/C catalyst decrease rapidly to 13 mA cm^{-2} and reached the pseudo steady state after a period of 15 s. PdCu/C catalysts also showed initial decay, but their current density decreased more slowly than that of Pd/C catalyst. After the application of the set potential for 60 s, the highest anodic current densities, 22 mA cm^{-2}, were measured on $Pd_{50}Cu_{50}$/C electrode, followed by $Pd_{25}Cu_{75}$/C (10.2 mA cm^{-2}), $Pd_{75}Cu_{25}$/C (10 mA cm^{-2}), and Pd/C (7 mA cm^{-2}). The $Pd_{50}Cu_{50}$/C catalyst shows the best catalytic performance among all four catalysts and Pd the lowest. Such results further demonstrated that the alloying of Cu can greatly improve the catalytic activity for the BH_4^- electrooxidation.

Table 1
Main performance parameters of DBFC using Pd/C and Pd–Cu/C catalyst.

Catalyst	Open circuit voltages (OCVs)	Current density (A cm^{-2})	Peak power density (mW cm^{-2})
Pd/C	1.0141	52	28
$Pd_{75}Cu_{25}$/C	1.0480	57	37
$Pd_{50}Cu_{50}$/C	1.1156	223	98
$Pd_{25}Cu_{75}$/C	1.0818	123	65

3.5. Fuel cell performance measurements

Fuel cell experiments were performed at 60 °C using Pd/C, $Pd_{75}Cu_{25}$/C, $Pd_{50}Cu_{50}$/C and $Pd_{25}Cu_{75}$/C as anode catalysts (0.5 mg metal cm^{-2}) and a commercial Pt/C cathode catalyst (0.5 mg Pt cm^{-2}). Fig. 7 shows the polarization (a) and power

Table 2
The comparison of DBFC performances using different anode electrocatalysts.

Anode	Cathode	Membrane	Anolyte	Catholyte	Power density (mW cm^{-2})	T (°C)	Mass activity basis (W g^{-1} anode catalyst)	Ref.
Pt–Ni/C(1:1) (5 mg metal cm^{-2})	Pt/C (4 mg Pt cm^{-2})	Nafion 117	0.5 M $NaBH_4$ + 2 M NaOH	O_2:flowrate: 1.25 l min^{-1}	53	60	10.6	[15]
Os/C (1 mg Os cm^{-2})	Pt black (4 mg Pt cm^{-2})	Nafion 117	2 M $NaBH_4$ + 2 M NaOH	O_2:flowrate: 0.2 l min^{-1}	69	60	69	[30]
Au–Pd/C(1:1) (5 mg metal cm^{-2})	Pt/C (4 mg Pt cm^{-2})	Nafion 117	2 M $NaBH_4$ + 2 M NaOH	O_2:flowrate: 0.2 l min^{-1}	47	60	9.4	[14]
$Au_{58}Ni_{42}$/C (0.9 mg metal cm^{-2})	Au/C (0.9 mg Au cm^{-2})	Nafion 117	1 M $NaBH_4$ + 3 M NaOH	2 M H_2O_2 + 0.5 M H_2SO_4	45.7	20	50.8	[20]
$Au_{67}Cu_{33}$/C (0.9 mg metal cm^{-2})	Au/C (0.9 mg Pt cm^{-2})	Nafion 117	1 M $NaBH_4$ + 3 M NaOH	2 M H_2O_2 + 0.5 M H_2SO_4	51.8	20	57.6	[21]
$Pt_{50}Cu_{50}$/C (0.9 mg metal cm^{-2})	Pt/C (0.9 mg Pt cm^{-2})	Nafion 117	1 M $NaBH_4$ + 3 M NaOH	2 M H_2O_2 + 0.5 M H_2SO_4	71.6	25	79.6	[18]
$Pd_{50}Cu_{50}$/C (0.5 mg metal cm^{-2})	Pt/C (0.5 mg Pt cm^{-2})	Nafion 115	1 M $NaBH_4$ + 6 M NaOH	O_2:flowrate: 0.2 l min^{-1}	98	60	196	This work

density (b) curves of a single DBFC operating with 1 M $NaBH_4$ and 6 M NaOH as a fuel and oxygen as an oxidant. Main performance parameters of DBFC such as open circuit voltages (OCVs) power density on the different anode catalyst are summarized in Table 1.

The open-circuit potential of the cell is approximately 1.1 V, which is lower than that of the standard cell potential for a DBFC operating on oxygen. A similar result has been also reported by Chatenet et al. [29]. The low potential is probably caused by mixed potential from simultaneous oxidation of BH_4^- ions and hydrogen at the anode side. All Pd–Cu/C catalyst showed higher OCV than Pd/C catalyst.

As shown in Fig. 7, the cell voltage of Pd/C anode catalyst dropped quickly with an increase in the current density. However, using Pd–Cu/C as the anode catalyst the cell voltage dropped much more slowly as the current density increased. All Pd–Cu/C catalysts exhibit higher electrochemical performance than Pd/C catalyst. And the fuel cell using $Pd_{50}Cu_{50}$/C as the anode catalyst gives the best performance, and the maximum power density is 98 mW cm^{-2} at a current density of 223 mA cm^{-2} at 60 °C, which is much higher than that of using Pd/C (28 mW cm^{-2}). Although the loading amount of Pd in $Pd_{50}Cu_{50}$/C is less 50% than that in Pd/C, the DBFCs using $Pd_{50}Cu_{50}$/C as anode catalysts shows three times better performance than that of Pd/C catalyst. The results show that the amount of copper up to fifty percent increases the catalytic activity synergistically. However, further increasing copper amount causes some drop in catalytic activity due to CuO formation as shown in CV results.

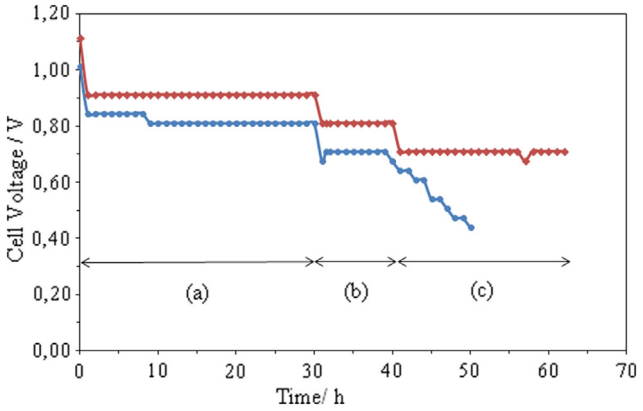

Fig. 8. Performance stability of the DBFC at 60 °C. Anode: $Pd_{50}Cu_{50}$/C and Pd/C. Anode catalyst loading: 0.5 mg metal cm^{-2}. Applied current density: (a) 20 mA cm^{-2} (b) 50 mA cm^{-2} and (c) 80 mA cm^{-2}. Other conditions are the same as in Fig. 7.

The comparison of DBFCs performances using different anode electrocatalysts in literature were summarized in Table 2. Comparing the results in Table 2, power output and mass specific activity of DBFC using $Pd_{50}Cu_{50}$/C as an anode catalyst is very high though Pd metal loading is 50% reduced and thus resulting in a much lower catalyst cost.

The stability of the materials under fuel cell conditions is particular importance from the point of view of practical application. Short-term stability of the DBFCs using $Pd_{50}Cu_{50}$/C and Pd/C as the anode electrocatalysts were tested by monitoring the cell voltage change with time at constant current density respectively. Three different current density, 20 mA cm^{-2}, 50 mA cm^{-2} and 80 mA cm^{-2} were applied to consecutive periods during 60 h. As shown in Fig. 8, the $Pd_{50}Cu_{50}$/C anode showed higher work voltage and better stability than Pd/C catalyst. At the current density of 80 mA cm^{-2}, Pd/C anode showed a rapid decrease in performance and stability in 10 h. On the contrary, $Pd_{50}Cu_{50}$/C anode maintained its high stability also at this current, indicating $Pd_{50}Cu_{50}$/C is a promising anode catalyst for the DBFC application.

4. Conclusion

In the present study, carbon-supported Pd and Pd–Cu bimetallic nanoparticles were prepared by a modified polyol method and used as anode catalysts for the DBFC. The Pd–Cu nanoparticles are uniformly dispersed on carbon support with average particle around 3.5 nm. Although Pd–Cu/C alloy catalysts show relatively low cost, they demonstrated much higher electrocatalytic activity than Pd/C for BH_4^- oxidation in DBFC. Among all studied electrocatalysts $Pd_{50}Cu_{50}$/C reveals the highest electrochemical performance. The maximum power density of DBFC using $Pd_{50}Cu_{50}$/C as the anode catalyst and Pt/C as the cathode catalyst was 98 mW cm^{-2} at 60 °C, while DBFC using Pd/C as the anode catalyst is only 28 mW cm^{-2}. Besides, the cell stability of DBFC using $Pd_{50}Cu_{50}$/C as the anode catalyst is much better compared with Pd/C catalyst. $Pd_{50}Cu_{50}$/C has the advantages of high performance, better stability and low-cost and could be a promising anode catalyst for the DBFC application.

Acknowledgments

The authors gratefully acknowledge Kocaeli University (Grant#: BAP 2010/12) for the financial support. Thanks are also to Dr. Özgür Duygulu for TEM measurements and to Mr. Aydın Canbaşa for his technical assistance.

References

[1] A.K. Shukla, C.L. Jackson, K. Scott, Bull. Mater. Sci. 26 (2003) 207.
[2] C. Ponce de Leon, F.C. Walsh, D. Pletcher, D.J. Browning, J.B. Lakeman, J. Power Sources 155 (2006) 172.
[3] J.H. Wee, J. Power Sources 155 (2006) 329–339.
[4] J. Ma, N.A. Choudhury, Y. Sahai, Renew. Sustain. Energy Rev. 14 (2010) 183–199.
[5] U. Demirci, F.G. Boyaci, T. Sener, G. Behmenyar, Actual. Chim. 306 (2007) 19–25.
[6] R.L. Pecsok, J. Am. Chem. Soc. 75 (1953) 2862–2864.
[7] J.H.H. Kim, S. Kim, Y.M. Kang, M.S. Song, S. Rajendran, S.C. Han, D.H. Jung, J.Y. Lee, J. Electrochem. Soc. 151 (2004) A1039–A1043.
[8] J.I. Martins, M.C. Nunes, R. Koch, L. Martins, M. Bazzaoui, Electrochim. Acta 52 (2007) 6443–6449.
[9] J.Q. Yang, B.H. Liu, S. Wu, J. Power Sources 194 (2009) 824–829.
[10] E. Gyenge, Electrochim. Acta 49 (2004) 965–978.
[11] E. Sanli, H. Celikkan, B.Z. Uysal, M.L. Aksu, Int. J. Hydrogen Energy 31 (2006) 1920–1924.
[12] B.H. Liu, Z.P. Li, S. Suda, Electrochim. Acta 49 (2004) 3097–3105.
[13] B.H. Liu, Z.P. Li, K. Arai, S. Suda, Electrochim. Acta 50 (2005) 3719–3725.
[14] M.H. Atwan, C.L.B. Macdonald, D.O. Northwood, E.L. Gyenge, J. Power Sources 158 (2006) 36–44.
[15] E. Gyenge, M. Atwan, D. Northwood, J. Electrochem. Soc. 153 (2006) A150–A158.
[16] A. Tegou, S. Papadimitriou, I. Mintsouli, S. Armyanov, E. Valova, G. Kokkinidis, S. Sotiropoulos, Catal. Today 170 (2011) 126–133.
[17] A. Tegou, S. Armyanov, E. Valova, O. Steenhaut, A. Hubin, G. Kokkinidis, S. Sotiropoulos, J. Electroanal. Chem. 634 (2009) 104–110.
[18] L. Yi, B. Hu, Y. Song, X. Wang*, G. Zou, W. Yi, J. Power Sources 196 (2011) 9924–9930.
[19] F. Pei, Y. Wang, X. Wanga, P. He, Q. Chen, X. Wang, H. Wang, L. Yi, Jia Guo, Int. J. Hydrogen Energy 35 (2010) 8136–8142.
[20] P. He, Y. Wang, X. Wang, F. Pei, H. Wang, L. Liu, J. Power Sources 196 (2011) 1042–1047.
[21] L. Yi, Y. Song, X. Liu, Xi. Wang, G. Zou, P. He, W. Yi, Int. J. Hydrogen Energy 36 (2011) 15775–15782.
[22] P. He, X. Wang, P. F, H. Wang, L. Yi, Int. J. Hydrogen Energy 36 (2011) 8857–8863.
[23] P. He, X. Wang, Y. Liu, X. Liu, L. Yi, Int. J. Hydrogen Energy 37 (2012) 11984–11993.
[24] N.N. Kariuki, X. Wang, J.R. Mawdsley, M.S. Ferrandon, S.G. Niyogi, J.T. Vaughey, D.J. Myers, Chem. Mater. 22 (2010) 4144–4152.
[25] M. Grdén, M. Lukaszewski, G. Jerkiewicz, A. Czerwinski, Electrochim. Acta 53 (2008) 7583.
[26] M. Simoes, S. Baranton, C. Coutanceau, J. Phys. Chem. C 113 (2009) 13369–13376.
[27] Y. Okinaka, J. Electrochem. Soc. 120 (1973) 739.
[28] V. Kiran, T. Ravikumar, N.T. Kalyanasundaram, S. Krishnamurty, A.K. Shukla, S. Sampatha, J. Electrochem. Soc. 157 (8) (2010) B1201–B1208.
[29] M. Chatenet, F. Micoud, I. Roche, E. Chainet, Electrochim. Acta 51 (2006) 5459–5467.
[30] V.W.S. Lam, E. Gyenge, J. Electrochem. Soc. 155 (2008) B1155–B1160.